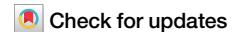
Published in partnership with CECCR at King Abdulaziz University



https://doi.org/10.1038/s41612-025-01072-2

# Declining summer circulation over the Eastern Mediterranean and Middle East



Harikishan Gandham<sup>1,2</sup>, Hari Prasad Dasari<sup>1,2</sup>, Thang M. Luong<sup>1,2</sup>, Raju Attada³, Waqar UI Hassan<sup>1,2</sup>, Prajeesh Athippatta Gopinathan<sup>1,2</sup>, Md Saquib Saharwardi<sup>1,2</sup> & Ibrahim Hoteit¹ ⊠

This study investigates the climatological and interdecadal (1980-2024) variations in summer (June-August) circulation over the Eastern Mediterranean and Middle East (EMME) using ERA5 global atmospheric reanalysis. The EMME summer climate is governed by the evolution of several key atmospheric circulation features: (1) High mean sea level pressure over the eastern Mediterranean (EM), along with a thermal low over the Arabian Peninsula (AP) and, (2) strong subsidence and downward advection of temperature in mid-troposphere centered over the EM, stretching into northern parts of Africa and AP. Diabatic heating released from ISM rainfall induces equatorially trapped westward-propagating Gill-type Rossby wave structure to its west. The interaction of this structure with the midlatitude westerlies gives rise to the aforementioned circulation features over the EMME. Our analysis reveals a substantial decline in the intensity of these circulation features over the study period, indicating an overall weakening of the summer circulation over the EMME. Further investigation points to a marked reduction in the subtropical westerly jet and the underlying westerlies during summer. This weakening may have contributed to reduced subsidence and a further decline in summer circulation strength over the EMME. Consequently, both Etesian winds over the EM and Shamal winds over the northern AP have shown notable declines in their occurrences. The weakened summer wind system has contributed to an abnormal increase in human-perceived temperatures and reduced dust activity.

The summers (June to August) in Eastern Mediterranean and Middle East (EMME) region are marked by high temperatures, minimal rainfall, and persistent dryness<sup>1,2</sup>. Within the EMME region, there are marked contrasts between the Eastern Mediterranean (EM) and Middle East (ME) climate. Inland areas of the ME frequently surpass 45 °C due to intense solar radiation, cloud-free skies, and strong adiabatic descent<sup>3,4</sup>, while the EM benefits from the moderating sea breeze advection<sup>5,6</sup>. Northerly winds called 'Etesians' in the EM<sup>7</sup>, help alleviate local high temperatures but also carry the polluted air originating over the Europe<sup>5</sup>. On the other side, 'Shamal winds' in the ME trigger dust storms, reducing visibility, lowering air quality, and impacting regional climate<sup>8</sup>. These prominent climatic conditions over the EMME are shaped by complex interactions among local topography, regional atmospheric circulation, and remote large-scale drivers<sup>2,9,10</sup>.

Summers in the EMME are marked by the retreat of Mediterranean low-pressure systems and the intensification of the subtropical high-pressure belt<sup>3</sup>. The Indian Summer Monsoon (ISM) system plays a

pivotal role in shaping the summer circulation over the EMME region<sup>11,12</sup>. Rodwell and Hoskins<sup>13</sup> (hereafter RH96) introduced the "Monsoon-Desert" mechanism, explaining how remote diabatic heating from the South Asian summer monsoon contributes to subtropical desert formation. In the framework proposed by RH96, intense convective activity associated with the ISM triggers westward-moving equatorially trapped Gill-type Rossby waves with a warm core structure, amplified under westerly zonal flow and weakened under easterly flow. As this warm structure expands north-westward, it creates steeper slopes in the isentropes over the EMME region, favoring subsidence when interacting with midlatitude westerlies along western and northern edges. A baroclinic Rossby wave structure forms, with an upper-level ridge and lower-level trough extending westward. Consequently, both subsidence and northerly flow over the EM emerge as integrated outcomes of Rossby wave dynamics induced by the ISM convection. Later Tyrlis et al. 10 leveraged ERA-Interim reanalysis to gain a more nuanced

<sup>1</sup>Physical Sciences and Engineering Division, King Abdullah University of Science and Technology (KAUST), Thuwal, Saudi Arabia. <sup>2</sup>Climate Change Center, National Center for Meteorology, Jeddah, Saudi Arabia. <sup>3</sup>Department of Earth and Environmental Sciences, Indian Institute of Science Education and Research Mohali, Punjab, India. —e-mail: ibrahim.hoteit@kaust.edu.sa

understanding of the EMME summer circulation dynamics and thermodynamics, particularly in relation to the ISM's influence.

The ISM exerts a strong influence on the diurnal, intra-seasonal, and interannual fluctuations of EMME circulations. Active monsoon conditions intensify Etesians<sup>14</sup>, while weak monsoon phases dampen Etesian strength, reduce ventilation, and contribute to heat waves over the EMME<sup>15</sup>. The seasonal peak in the strength of the Etesian and Shamal winds and associate dust activity coincides with the peak phase of ISM activity<sup>7,16</sup>. The ISM's interannual variability affects the EMME climate notably, with strong ISM phases enhancing subsidence, which in turn strengthens the Etesian and Shamal winds<sup>3,11</sup>. Coupled model projections suggest that future increases in South Asian monsoon activity could intensify subsidence over the EMME, potentially amplifying the arid conditions<sup>12</sup>. The EMME is already prone to extreme temperatures<sup>4,17,18</sup>, droughts<sup>19,20</sup>, and frequent dust and air pollution events<sup>21-24</sup>. These factors significantly impact air quality, public health, and the economies of the region. Under these sensitive conditions, any major shifts in summer circulation over the EMME could significantly influence extreme weather events.

In this regard, the present study aims to examine the climatology and trends (1980–2024) in the summer circulation over the EMME region, using the ERA5 global atmospheric reanalysis. The structure of the paper is as follows: Section 2 presents and discusses the results. Section 3 concludes the present study, and Section 4 of this paper delineates the data and methodology of the study.

#### Results

#### Climatological features of summer circulation over EMME

The summer Mean Sea Level Pressure (MSLP) (Fig. 1a) patterns are characterized by an evolution of contrasting pressure zones over the EM and ME. The high-pressure centered over the EM, with intensity of 1014 hPa, distributed further westward. Meanwhile, a pronounced thermal low is witnessed over the AP. This thermal low, often referred to as the "Arabian heat low," forms due to intense surface heating<sup>25</sup>. The observed significant east-

west pressure gradient between these contrasting pressure regimes favor a cross equatorial flow (Fig. 1a) that sweep down from the Mediterranean towards the southeast regions. These winds are locally known as the "Etesians" in the EM region<sup>26</sup>. Further, the existing pressure gradient establishes strong northwesterly "Shamal winds"<sup>16,27</sup> across the AP, channeling through the Tigris-Euphrates basin into the Kingdom of Saudi Arabia (KSA).

Figure 1b illustrates the climatological summer spatial distribution of the  $\omega$  values at the 500 hPa pressure level. The broad area of strong positive  $\omega$ values over EMME region suggest substantial subsidence extending from EM to the AP. As discussed earlier, several studies indicated that ISM induced Rossby wave pattern facilitates the formation of this subsidence zone through its interaction with the westerlies over the region. The meridional mean ω depicts strong subsidence throughout the tropospheric column over the EMME, with the maximum magnitudes located at midtropospheric levels (Figure S1a). The zonal circulation features depicted using the  $\omega$  and wind vector  $(u, -\omega)$  reveal several interesting features. At the high-altitude areas of the EM, the meridional wind contribution to the total wind speed is minimal, making the zonal component the primary driver of the overall wind pattern. Further, just below the core of the subtropical westerly jet, the wind vectors begin to tilt more steeply downward, suggesting that the sinking air to the west of 30°E, which could be due to the prevailing zonal westerlies at these levels.

Figure 1b also indicates strong upward motions  $(-\omega)$  around the Zagros Mountain Range (ZMR) and the southwestern AP region, while a pronounced descent occurs over Iraq and the Arabian Gulf regions. These strong vertical motions over the ZMR are steered by thermal and mechanical forcings<sup>28</sup>. As an elevated heat source, the ZMR induces upward air movement due to intense solar heating, forming a mid-tropospheric anticyclone, known as the Iran Anticyclone. This thermal forcing causes convergence at surface and enhances the vertical advection. Additionally, the ZMR's topography interacts with lower tropospheric summertime easterlies, further intensifying upward motion. This upward advection over

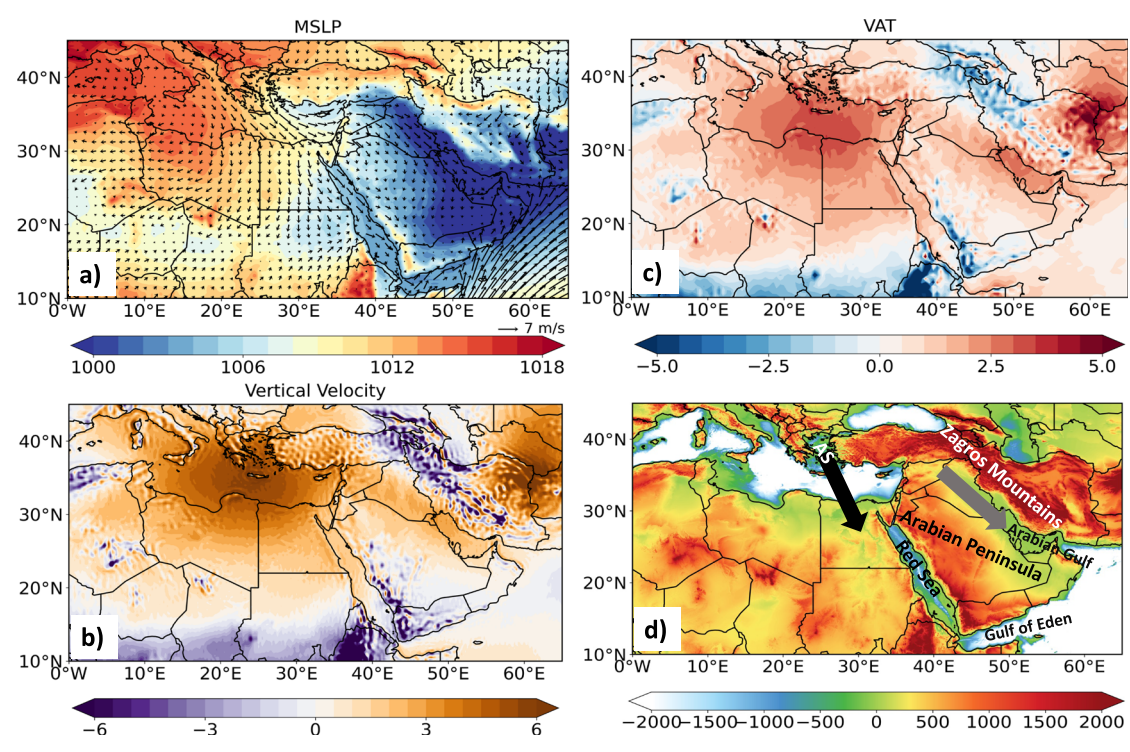


**Fig. 1** | Key factets of the summer circulation over the EMME. Summer climatology of (a) Mean sea level pressure (shaded; units: hPa) and 10-meter winds (vectors; unit: m/s), (b) vertical velocity at 500 hPa level (units: Pa/min), (c) vertical temperature advection (units: K/day) averaged during the period 1990–2019, and

(d) topography (shaded; units: meters) map of EMME region indicating conceptual positions of Etesian winds (black arrow), Shamal winds (grey color arrow), and Aegean Sea marked as 'AS'.

the ZMR promotes a distinct descent to its west, leading to pronounced subsidence over the northeastern AP, extending across the Mesopotamian plains to the Arabian Gulf<sup>29</sup>.

Here, we further examine the thermal structure of the troposphere by analyzing the seasonal distribution of the temperature tendencies over the EMME. The VAT distribution at 500 hPa reveals a region of positive values over the EMME (Fig. 1c). On a seasonal scale, VAT dominates the temperature advection processes, counteracting the cooling effect induced by horizontal advection of temperature (Figure not shown) over the EMME. The analysis of longitude-pressure cross-sections of VAT in the EMME (Figure S1b) region reveals positive VAT values stretching between the 500 and 200 hPa levels, indicating subsidence-induced warming driven by the ISM. This VAT pattern

contributes to the development of a warm core structure, especially in subsidence regions where downward air movement induces adiabatic warming. Consequently, the EMME region emerges as a mid-tropospheric hotspot during boreal summers.

#### Trends in summer atmospheric circulation over the EMME

In Fig. 2, we disclose the long-term trends in the summer circulation features over the EMME. MSLP is showing a significant weakening tendency across much of the EM, extending into northeastern Africa (Fig. 2a). The trend values in these areas reach up to  $-0.5\,\mathrm{hPa}$  per decade (p-value < 0.05), with a significant pressure drop is centred over western Turkey, spanning the Aegean and Mediterranean Seas. Moreover, the negative MSLP trend shows a more pronounced westward extension from the Aegean Sea. These areas

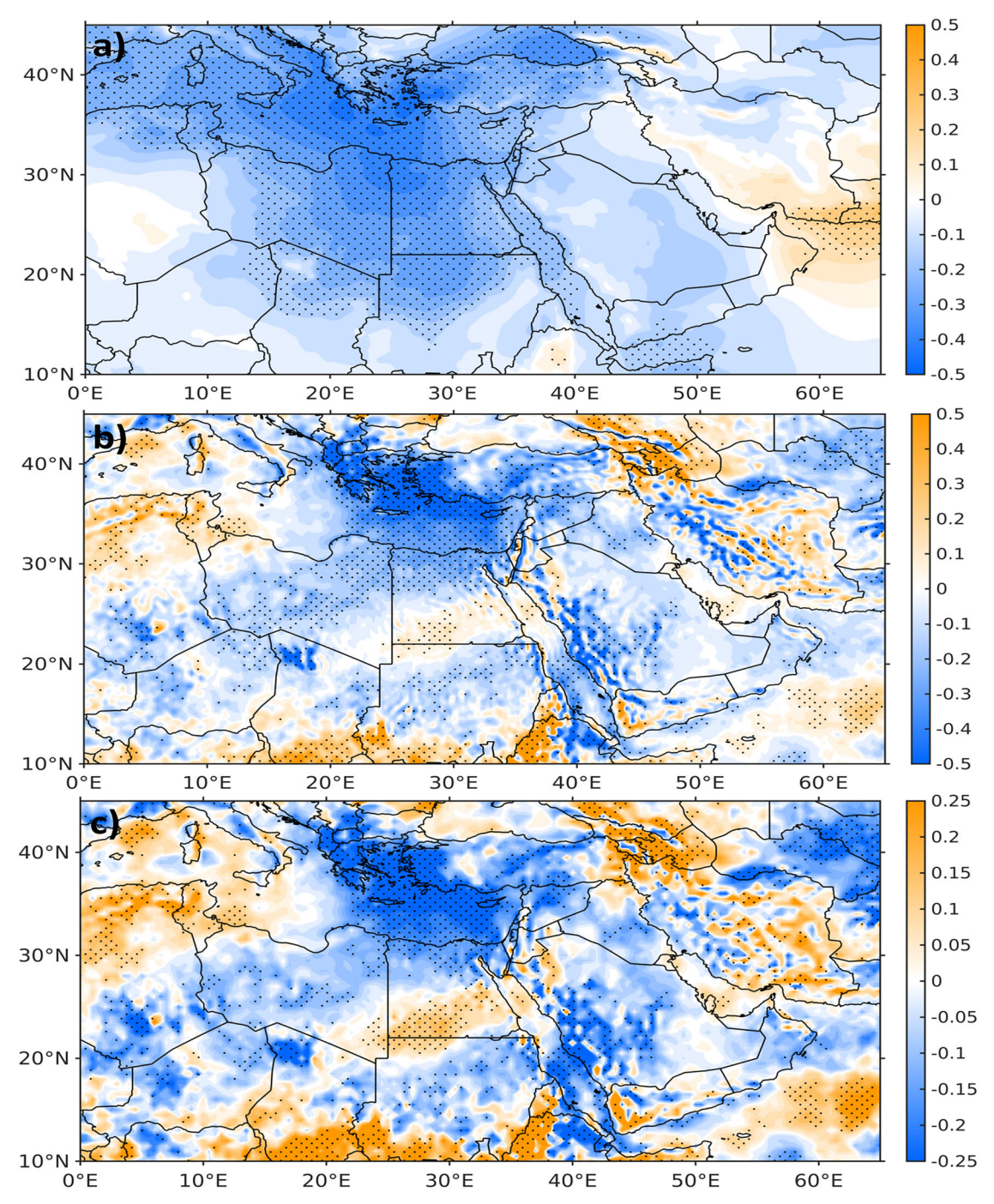


Fig. 2 | Temporal evolution of summer circulation over the EMME. Long-term trends (1980—2024) in the summer mean (a) Mean Sea level pressure, (b) vertical velocity at 500 hPa, and (c) vertical temperature advection at 500 hPa. The regions with p-value < 0.05 are indicated by the dots.

lie at the periphery of the summer high-pressure system centred further west (Fig. 1a). In contrast, the thermal low over the AP and Arabian Gulf regions remains stable, compared to the high-pressure zone over the EM. Figure 2b shows the long—term trends in summer mean ω at 500 hPa. A significant trend toward weaker subsidence is evident over the EM and North Africa regions. Further verification of the trends in meridional mean  $\omega$  (Figure S2a) indicates a marked reduction in subsidence throughout the tropospheric column confined to the region between 20°E and 30°E. This consistent decline in subsidence strength can potentially impact VAT tendencies. This is noticeable in Fig. 2c, which shows the spatial patterns in mid-tropospheric VAT distribution across the EMME, highlighting a notable decline in the downward advection of temperature over the region. Interestingly, the trend patterns in VAT over the EMME largely mirror those observed in ω. Moreover, the decreasing trends in  $\omega$  and VAT align well with the observed decreases in MSLP, suggest reduced subsidence and warm core promoting the lowering of surface pressure.

We also examined trends in the summer circulation features over the EMME region using the MERRA2 and NCEP2 reanalysis datasets (Figure S3). The analysis confirmed a similar weakening of summer circulation features across both datasets. The MERRA2 results (Figure S3a—c) showed closer agreement with the previously used ERA5 reanalysis. NCEP2 (Figures S3d—e) exhibited a broader decline in summer circulation, though with regional discrepancies relative to the higher-resolution datasets.

## Factors driving the weakening of summer circulation over the FMMF

The abnormal changes observed in the summer climate across the EMME suggest a possible influence of ISM variability. To verify this, we first analyzed summer mean vertical velocities averaged over the ISM region (70-90E; 5-25 N) and present the results in Fig. 3 (red line). The time series reflects a prominent interannual and decadal variability in the ISM activity, with a phase of weakening until 2002, followed by a strengthening during the subsequent period. This resurgence in summer monsoon activity is linked to a favorable land-ocean temperature gradient, driven by pronounced warming over the Indian subcontinent alongside slower warming over the Indian Ocean 30-32. Such variability in the ISM would typically elicit parallel responses in the EMME climate. Surprisingly, however, ω averaged over the EM region (17-31E; 30-41 N) shows a consistent declining trend (Fig. 3; blue line), indicating weakening subsidence without any pause or reversal. Through this analysis, we confirm the development of a marked asynchrony between the remote influencer (ISM) and the passive receiver (EMME), characterized by strengthening monsoonal ascent over the ISM and weakening subsidence over the EMME region. This distinct shift in the relation suggests that the EMME's reliance on the ISM's influence may be eroding, or some other atmospheric dynamics moderating the EMME climate independently of ISM variations.

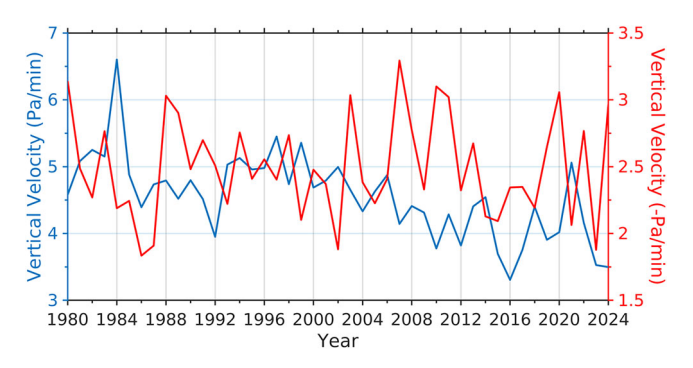


Fig. 3 | Long-term trends (1980–2024) in the vertical velocities averaged (at 500 hPa) over eastern Mediterranean (30–41E, 17–31 N; blue line) and Indian summer monsoon region (70–90E, 5–25 N; red line). The left y-axis indicates the subsidence motion, while the right y-axis represents the upward motion, which is multiplied by -1 for better representation.

Controlled numerical experiments are particularly valuable for isolating and confirming the causative role of the ISM variability in shaping EMME summer climate. Foundational studies such as RH96<sup>13</sup>, along with subsequent idealized simulations, have demonstrated the effectiveness of simplified frameworks in diagnosing atmospheric responses to diabatic heating. Later, Watanabe and Kimoto<sup>33</sup> developed a Linear Baroclinic Model (LBM), which has since been widely employed to understand the impact of diabatic heating on large-scale circulation patterns<sup>34–38</sup>. Notably, Cherchi et al.<sup>11</sup> employed the LBM to examine the influence of ISM-related heating on EMME circulation and highlighted the sensitivity of subsidence over the region to both the horizontal distribution of monsoonal rainfall and the vertical structure of diabatic heating over ISM region. Their analysis was further extended to explore potential future changes in this teleconnection based on CMIP6 projections<sup>12</sup>. Motivated by our findings and informed by this earlier work, we plan to conduct similar idealized simulations to assess how temporal shifts in ISM strength and heating profiles affect summer subsidence and circulation over the EMME region.

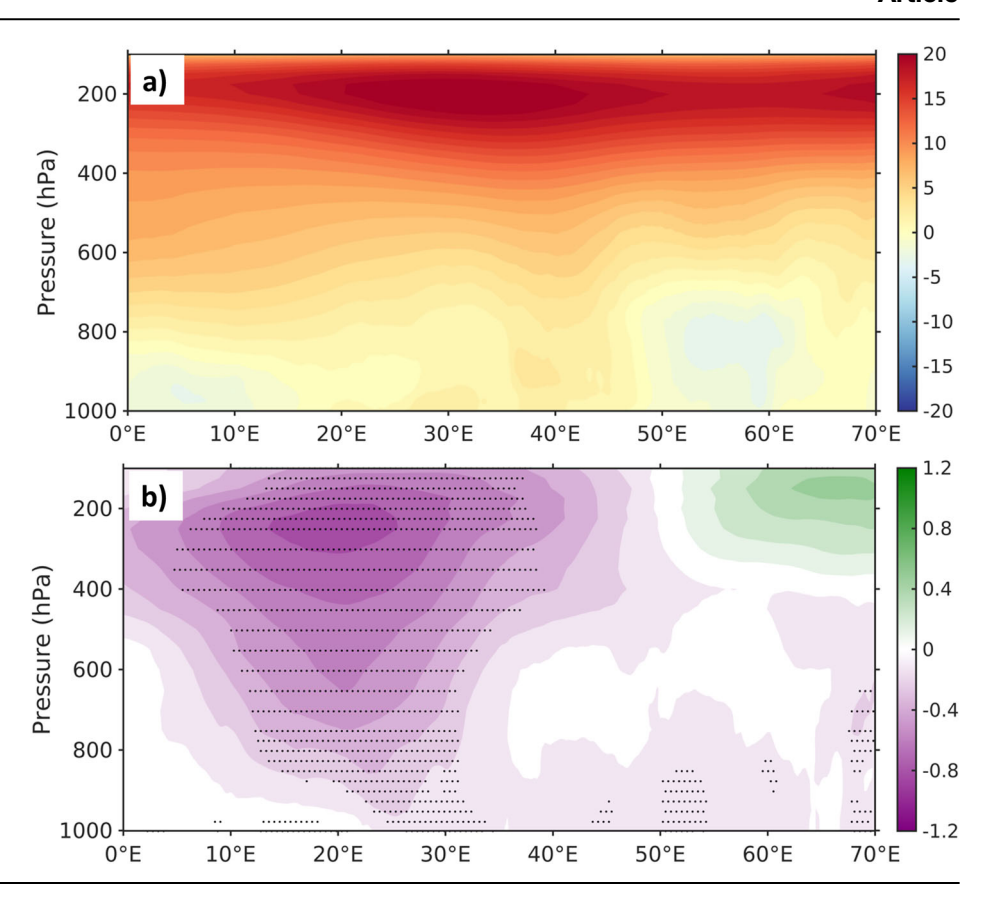
Tyrlis et al. <sup>10</sup> indicated that the midlatitude westerlies interact with the warm upper-level structure induced by ISM-triggered Rossby waves over the EMME region. This interaction strengthens the tropospheric subsidence, a pattern clearly identified in our analysis (Figure S1b). Therefore, it is anticipated that any changes in this zonal westerlies could impact the  $\omega$  patterns. To investigate this, we examined the climatological summer distribution of the meridional mean zonal winds over the EMME region (Fig. 4a). We noticed dominance of westerlies throughout the troposphere, with high wind speeds >20 m/s above 300 hPa, representing the subtropical westerly jet. The trend in zonal winds is showcased in Fig. 4b, with the most pronounced reduction limited to EMME longitudinal belt. Besides, the most significant weakening is observed in the upper-level westerlies (above 300 hPa). This indeed suggests a significant decline in the strength of subtropical westerly jet, a trend noted in several recent studies  $^{39,40}$ .

The Detection and Attribution Model Intercomparison Project (DAMIP) model attribution studies have shown that anthropogenic aerosol emissions have contributed to significant weakening in the summer subtropical jet over the past four decades<sup>41</sup>. Aerosol-induced cooling in the Tropics, along with warming in mid-to-high latitudes, has decreased the meridional temperature gradient. Through thermal wind balance, this reduction in the temperature gradient leads to the decrease in the vertical shear of the zonal winds and weakening the subtropical jet. Consequently, this substantial reduction in westerly strength may have weakened subsidence and subsequent VAT. Importantly, the surface high-pressure system, sustained by strong tropospheric subsidence, has also significantly weakened.

Internal decadal climate variability modes, such as the Atlantic Multidecadal Variability (AMV) and Pacific Decadal Oscillation (PDO), could also potentially influence summer circulation changes over the EMME region. Additionally, variability in Arctic sea ice concentrations might affect regional atmospheric circulation patterns. We have further analyzed the influence of these factors on the observed changes in EMME summer circulation. To do this, we calculated the summer mean values of each climate mode index used in the analysis. We first analyzed the association between the low-frequency climate mode, Atlantic Multidecadal Variability (AMV)<sup>42</sup>, and summer circulation of the region (Figures S4a-c). Correlation analysis indicated strong negative associations between AMV and key circulation variables. Given that the AMV has been predominantly positive phase in recent decades, this negative correlation aligns with observed weakening trends in summer circulation over the region. Areas exhibiting substantial declines in circulation demonstrated strong (r > 0.7) and statistically significant correlations with the AMV. AMV has been shown to influence the weakening of the subtropical westerly jet<sup>43-47</sup>, thereby affecting the summer circulation over the EMME region.

Next, we examined the association between Arctic Sea Ice Concentrations (SIC) averaged over 10°W–60°E and 70°N–80°N region<sup>48</sup>, and summer circulation over the EMME region (Figures S4d–f). Interestingly, SIC exhibited a positive correlation with the region's summer circulation.

Fig. 4 | Vertical distribution of zonal westerlies during summer. Longitude-pressure cross sections of zonal westerlies averaged over EMME region (31–40°N) (a) summer climatology of zonal westerlies (units: m/s) averaged during 1990–2019, and (b) long-term trends in zonal westerlies (units: m/s per decade) over the study period (1980–2024). The dots in the second figure indicates the trends with *p*-value < 0.05.



During the analysis period, SIC has shown a consistent declining trend, particularly during the summer months, contributing to enhanced warming in higher latitudes<sup>49,50</sup>. This warming reduces the equator-to-pole thermal gradient and subsequently may weakens summer circulation by altering the strength of midlatitude westerlies.

Lastly, we explored the relationship between the Pacific Decadal Oscillation (PDO) and summer circulation over the EMME. The PDO is a long-term oscillation over the Pacific Ocean, typically spanning 20 to 30 years. Similar to SIC, the PDO exhibited a positive correlation with key summer circulation variables. In summary, the combined influence of AMV, SIC, and PDO provides important insights into the external drivers modulating EMME summer circulation. Among them, AMV emerges as a key contributor to the observed long-term weakening, acting through its influence on the westerlies and subtropical westerly jet.

### Implications of the diminished summer circulation over the EMME

In this section, we examine the implications of the weakening EMME summer circulation on local wind regimes, human-perceived temperatures, and dust activity.

Impacts on the surface winds. The pressure gradient between EM's high-pressure and low-pressure over the eastern AP drives local wind patterns. Figure 5 shows the time series of summer mean MSLP, averaged over the EM (red line) and eastern AP (blue line), along with the difference between these two regions (black line). Apart from the strong interannual variability, the pressure difference between the EM and AP shows a consistent declining trend throughout the study period, with an average rate of 0.5 hPa per decade. Further, decline is most pronounced during the years 2000 to 2024. As discussed in Section 2.2, the high-pressure over the EM has weakened significantly during the recent decades. This indeed contributes to the observed decrease in the pressure gradient depicted in Fig. 5, which favors the weakening of local wind

patterns. To substantiate these changes, we further analyze the mean climatology and trends of the 10-meter horizontal wind components (Fig. 6). Figure 6a illustrates the broader reach of the westerlies, with a primary branch creating a dominant flow over the EM and northern AP, while a secondary branch extends southward along the Red Sea. In the recent decades, these westerlies show a notable decline over Arabian Gulf and central-west and southern KSA, compared to moderate decreases across the Red Sea basin (Fig. 6d). The analysis of the meridional component (Fig. 6b), we have found that the northerly winds prevail across most of the EMME region. The core region of northerlies noticed over the Aegean Sea and stretches southward into north Africa mainly Egypt and Libya. Recent decades experience a diminishing trend in northerlies over EM and Egypt (Fig. 6e), with similar declines also observed over the northwestern AP, Arabian Gulf<sup>51</sup>, and southeastern KSA. The surface wind climatology across the EMME region highlights distinct patterns. Figure 6c shows that wind speeds reach up to 7 m/s over the northeastern AP, with stronger winds over the Mediterranean and northern Red Sea. On land, Egypt experiences notable decreases followed by west-central and northwest regions of the AP. Over oceanic regions, substantial reductions are evident throughout the eastern Mediterranean Sea, Red Sea, and Arabian Gulf. The overall decline in wind speeds suggests a potential reduction in the frequency of EW and SW episodes.

We now examine the climatological characteristics and trends of these wind episodes in detail. EW and SW episodes are identified based on the methodology outlined in Section 4.3. Figure 7a illustrates the distribution of EW and SW episodes during EMME summers. The highest frequency of EW episodes is concentrated over the Aegean Sea and EM, reaching up to 60 events per season. On the other hand, SW episodes extend from Syria through Iraq to the Arabian Gulf, with an eastward extension limited by the ZMR. The frequency of SW episodes reaches up to 40 events per season, making them slightly less frequent than EW episodes. The methodology also identifies a notable band of frequent wind episodes in other regions. For example, a distinct maximum appears along the Iran-Afghanistan border,

representing high-intensity 'Levar wind' events<sup>52</sup>. Secondly, we also noticed a band of persistent wind episodes along the Red Sea, running north to south. Figure 7b outlines the spatial trends in the occurrence of EW and SW events across the EMME region. The EW episodes across much of the EM experience a significant decline, with a trend value of approximately -2 events per decade. Concurrently, a marked decline in SW events spans the Tigris-Euphrates river basin and extends into the Arabian Gulf.

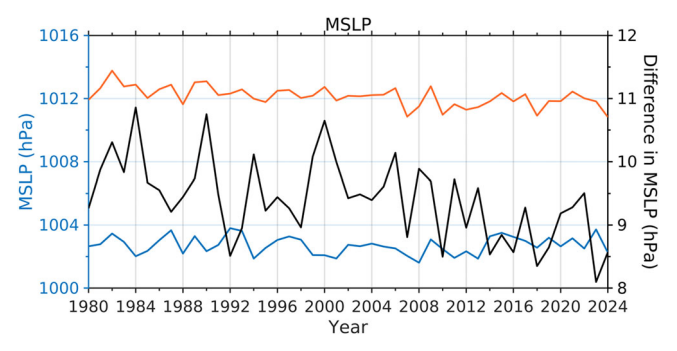


Fig. 5 | Long-term trends (1980–2024) in the summer mean MSLP averaged over the eastern Mediterranean high pressure (30–41E, 17–31 N; red line) and Arabian heat low (45–60E, 15–35 N; blue line), along with the difference between the two regions (black line).

The observed reduction in surface winds, resulting in declining frequencies of EW and SW episodes, has significant implications for local dust activity. Specifically, the wind speeds of Shamal episodes are critical for initiating dust emissions across the AP<sup>16</sup>. The analysis of summer mean dust column density from 2000 to 2024 reveals a moderate decline in dust activity across the Tigris-Euphrates region, coinciding with a substantial weakening of SW episodes (Figure S5). We believe that this decline in wind-driven dust activity appears to be partially offset by the intensification of local megadrought conditions<sup>53</sup>. The prolonged droughts have amplified local dry soil conditions, enabling dust emissions at sub-critical wind speeds and sustaining dust activity despite weaker local wind speeds.

Impact on the human-perceived temperatures. Figure 8 illustrates the summer climatology and long-term trends of AT across the study region. Figure 8a reveals elevated AT values over the eastern AP and the Red Sea, with magnitudes reaching up to 45 °C, driven by intense surface heating and high humidity. In contrast, the north-central AP exhibits moderate AT values. The EM and its downwind regions show relatively lower AT values compared to the AP. A distinct gradient in AT observed between the EM and ME regions. The long-term trends show (Fig. 8b) an abnormal AT increase of approximately 0.8 °C per decade (*p*-value < 0.01), particularly over the EM, north-central AP, and Egypt, where AT exhibits moderate values during summer. Surface temperature and vapor pressure trends in these areas further confirm the conditions driving the increase of AT. The analysis of surface temperatures indicates a

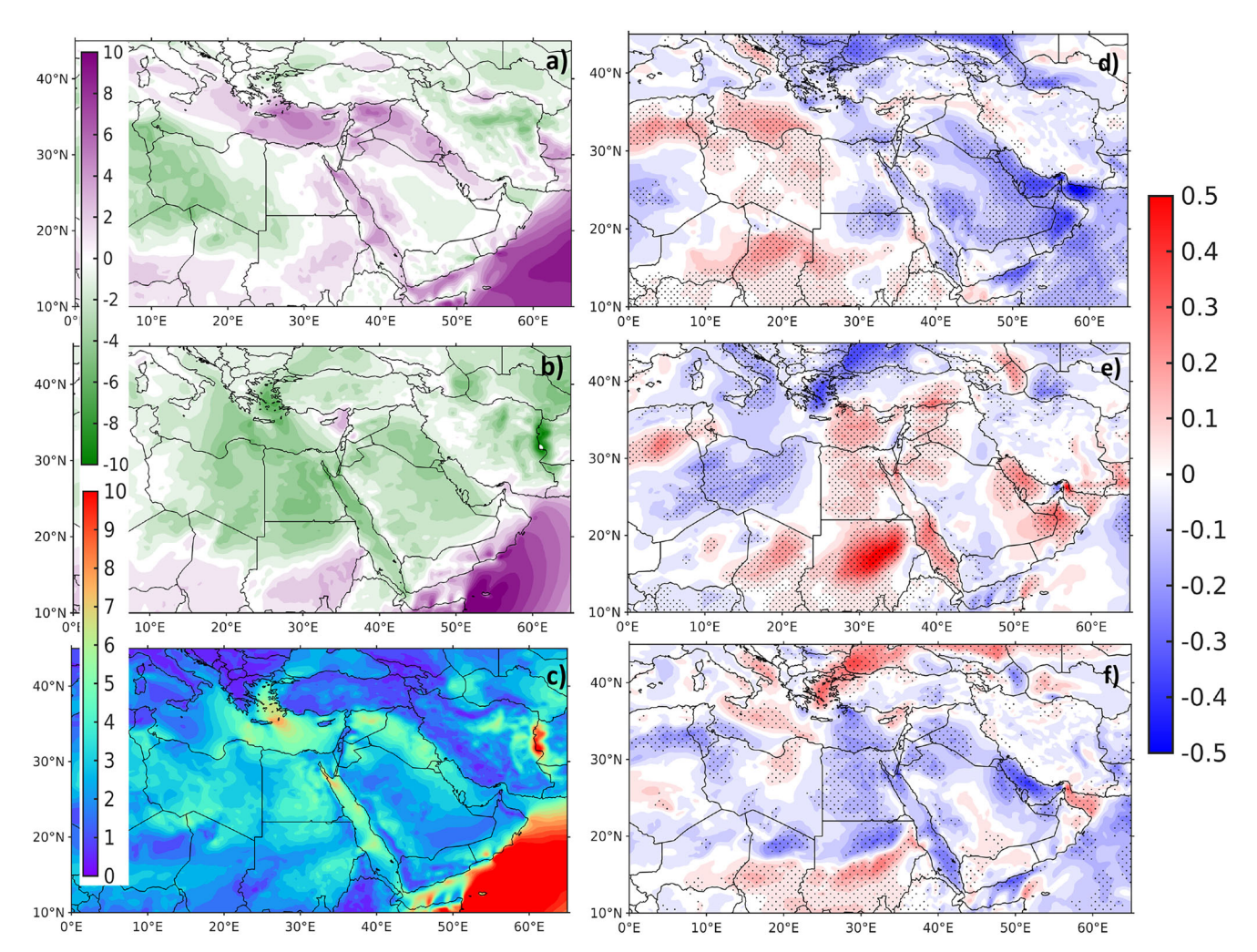
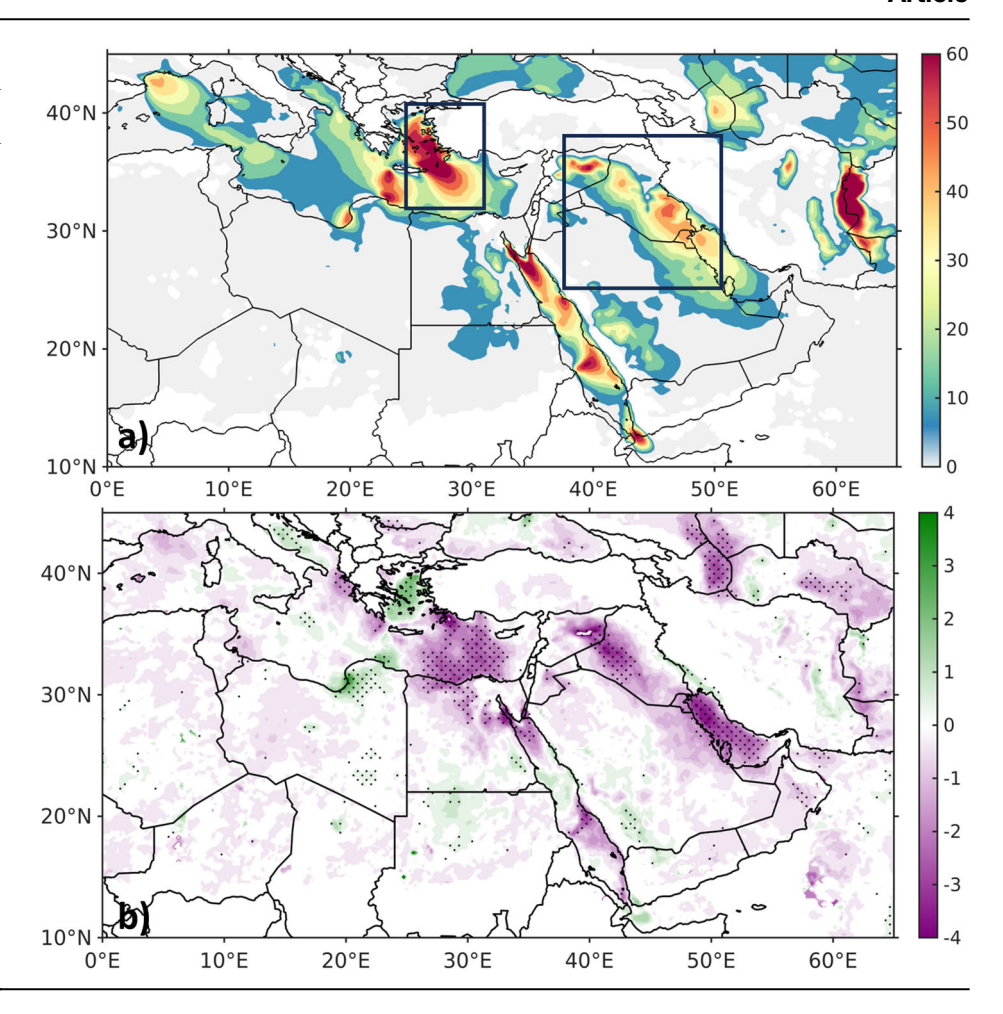


Fig. 6 | Key characterstics of summer surface winds over the EMME. Summer season climatology of 10-meter (a) zonal winds (units: m/s), (b) meridional winds (units: m/s), (c) wind speeds (units: m/s) averaged during 1990–2019. Trends in

summer mean (**d**) zonal winds (units: m/s per decade), (**e**) meridional winds (m/s per decade), and (**f**) wind speeds (m/s per decade) during the period 1980 to 2024, with dots indicating statistically significant trends (p-value < 0.05).

Fig. 7 | Prominent summer wind regimes over the EMME. a Summer climatology of Etesian (small box) and Shamal (large box) wind events (units: days), averaged over the period 1990–2019. b Spatial trends of these wind events (units: days/decade) from 1980 to 2024. The dots in the second figure indicate the trends with *p*-value < 0.05.



pronounced increase over regions experiencing significant AT rises (Fig. 8c). In contrast, vapor pressure shows moderate increases across the EMME, with oceanic regions, emerging as hotspots for higher atmospheric moisture levels (Fig. 8d). Moreover, the observed increase in AT coincides with a significant decline in wind speeds, especially over hotspots of warming, highlighting the role of reduced ventilation on thermal heat stress. The substantial reduction in wind speeds across the EM and adjacent areas has diminished the natural cooling effect provided by ventilation, further amplifying AT levels. Thus, the combined impact of rising local temperatures and weakening winds has driven abnormal AT trends, resulting in a significant increase in heat stress.

#### Discussion and conclusion

This study examined the prominent aspects of the summer circulation and their changes over the Eastern Mediterranean and Middle East (EMME) region from 1980 to 2024, utilizing ERA5 global atmospheric reanalysis data. The key findings of this work can be summarized as follows:

- 1. The summer surface climate over the EMME is shaped by the establishment of high pressure over the eastern Mediterranean (EM) and a thermal low over the Arabian Peninsula (AP), resulting in a strong east-west pressure gradient that drives cross-equatorial flow. Subsidence dominates the EMME troposphere, peaking below 300 hPa, enhancing adiabatic warming. Sinking motions also advect heat downward, influencing the troposphere's thermodynamics and making EMME a mid-tropospheric hotspot. Indian Summer Monsoon convection drives these patterns through inducing a westward-propagating Rossby waves.
- Our analysis indicates a continuous decline in surface high pressure, subsidence motions, and downward temperature advection over the EMME, pointing to an overall weakening of the summer circulation in

- this region over the study period. Concurrently, the strengthening of ISM activity during recent decades suggests a diminishing connection between these coupled climate phenomena.
- Critical analysis reveals a significant weakening in the subtropical westerly jet and the underlying westerlies over the study period. This reduction could predominantly weaken tropospheric subsidence, resulting in diminished downward temperature advection and weakened surface high pressure over the EMME region.
- Analysis highlights that the weakening EMME summer circulation has reduced the east-west pressure gradient between the EM and AP, destabilizing northerly wind patterns and leading to further reductions in horizontal wind speeds across the EMME.
- As a result, both Etesian wind episodes across the EM and Shamal wind episodes over the Tigris-Euphrates region have weakened, leading to reduced dust activity, particularly over the northern AP.
- Additionally, these weakened wind conditions have contributed to abnormal positive trends in apparent temperature, significantly intensifying heat stress in the region.

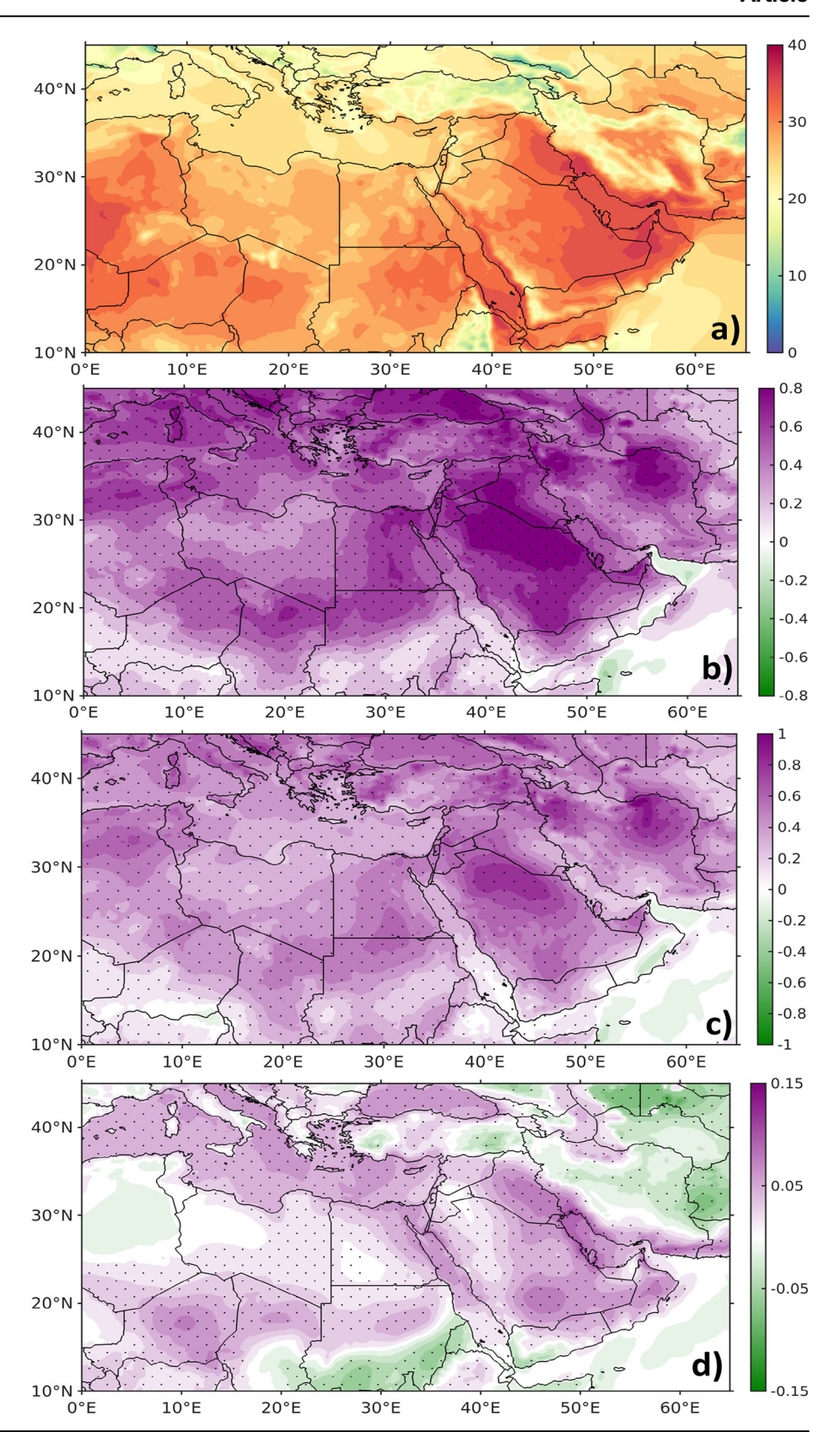
The results of this study highlight a marked weakening of the EMME summer circulation from 1980 to 2024, significantly affecting wind regimes, thermal discomfort, and dust activity across the region. This knowledge is vital for understanding future projected changes in the EMME summer climate, assessing their broader impacts, and developing strategies to mitigate climate extremes.

### Data and Methods

#### Data

We use daily means of several atmospheric variables available at a  $0.25^{\circ} \times 0.25^{\circ}$  resolution from the ERA5 global reanalysis<sup>54</sup> to examine key

Fig. 8 | Distribution of surface temperature and human-discomfort over the EMME. a Summer climatology of apparent temperature (units: °C), averaged over the period 1990–2019. Spatial trends in (b) apparent temperature (units: °C /decade), (c) surface temperatures (units: °C /decade), and (d) vapor pressure from 1980 to 2024. The dots indicate the trends with *p*-value < 0.05.



summer circulation features and their variations over recent decades in the EMME region. Hourly 10-meter horizontal wind data were utilized to identify Etesian and Shamal wind events. Additionally, hourly surface air temperature and dewpoint temperature were analyzed to compute indices of thermal discomfort. To assess the robustness of the observed trends in

summer circulation, we also examined additional global reanalysis datasets, including NCEP2 ( $2.5^{\circ} \times 2.5^{\circ}$  resolution) and MERRA2 ( $0.5^{\circ} \times 0.625^{\circ}$  resolution). We utilize the monthly mean dust column mass density available at a  $0.5^{\circ} \times 0.625^{\circ}$  resolution from the MERRA2 global aerosol reanalysis<sup>55</sup>.

#### Characterization of the thermodynamic state of the troposphere

The analysis of the thermodynamic state of the troposphere over the EMME involves quantifying the terms in the thermodynamic energy equation, expressed in isobaric coordinate system, as follows<sup>56</sup>:

$$\frac{dT}{dt} = \frac{J}{C_p} - w \frac{T}{\theta} \frac{\partial \theta}{\partial p} + \left( -u \frac{\partial T}{\partial x} \right) + \left( -v \frac{\partial T}{\partial y} \right) \tag{1}$$

where T is temperature,  $\theta$  is potential temperature, u and v are the horizontal wind components,  $\omega$  is the vertical velocity, J is the diabatic heating rate, and  $C_P$  is the specific heat of dry air at constant pressure. The term  $\frac{dT}{dt}$  represents the Local Temperature Tendency (LT), while  $\frac{I}{C_P}$  represents the Total Physics Temperature Tendency (TPT). The term  $-w\frac{T}{\theta}\frac{\partial\theta}{\partial\rho}$  represents the Vertical Advection Temperature Tendency (VAT), whereas  $-u\frac{dT}{dx}$  and  $-v\frac{dT}{dy}$  denote the temperature tendencies due to zonal advection (ZAT) and meridional advection (MAT), respectively. The combined effect of ZAT and MAT corresponds to the horizontal advection temperature tendency (HAT). Both HAT and VAT describe temperature tendencies due to adiabatic processes, while TPT reflects the diabatic heating term. Thus, Eq. (1) represents the local total temperature change as the result of both diabatic and adiabatic processes.

#### Identification of Etesian and Shamal wind episodes

The detection of Etesian and Shamal wind episodes was performed at each ERA5 grid point. We applied a common set of criteria to the hourly wind data to identify these events. First, we identified hours when hourly wind speeds exceeded 7 m/s and wind directions ranged between 270° and 30°, corresponding to northwesterly to north-northeasterly winds. A day was classified as an Etesian or Shamal wind day at a given grid point if these conditions were met for at least 6 hours within that day<sup>7,16,27</sup>. Finally, we estimated the frequency of EW and SW days during the summer season at each ERA5 grid point.

#### **Human-perceived temperature**

Human-perceived temperature (HPT) refers to the temperature that a person feels, rather than the actual air temperature measured by a thermometer<sup>57</sup>. Apparent temperature (AT) is a crucial indicator for HPT, incorporating factors such as air temperature, humidity, and wind speed<sup>58-61</sup>. AT provides a robust measure of thermal comfort and stress, making it essential for assessing heat-related health risks, particularly during extreme weather events<sup>62</sup>. Here, AT is calculated based on the formula used in Steadman (1984)<sup>58</sup>.

$$AT = -2.7 + 1.04T + 2.0vp - 0.65u$$
 (2)

where T is 2 meter air temperature in degrees Celsius, and u is wind speed (m/s) at 10 meter level. Here vp is vapor pressure calculated using the dewpoint temperature (Td) at 2 meter based on the Magnus formula<sup>63</sup>.

$$vp = 0.6112 \times exp\left(\frac{(17.67 \times Td)}{(Td + 243.5)}\right)$$

Trends were computed using the least-squares linear regression method. Statistical significance of these trends was assessed with a two-tailed Student's t-test.

#### Data availability

ERA5 dataset is obtained from the CDS server (https://cds.climate.copernicus.eu/#!/home). Monthly mean dust column load is downloaded from the Giovanni website (https://giovanni.gsfc.nasa.gov/giovanni/). We downloaded the NCEP2 dataset from the PSL website (https://psl.noaa.gov/data/gridded/data.ncep.reanalysis2.html). We retrievedthe MERRA2 obtained from the GESDISC server (https://disc.gsfc.nasa.gov/datasets? keywords=MERRA-2&page=1). We obtain the Atlantic multidecadal variability data from the NCDC server (https://www1.ncdc.noaa.gov/pub/

data/cmb/ersst/v5/index/ersst.v5.amo.dat). We used pacific decadal oscillation data hosted by NCEI (https://www.ncei.noaa.gov/pub/data/cmb/ersst/v5/index/ersst.v5.pdo.dat). Finally, we downloaded Arctic Sea Ice concentrations from the CDR (https://nsidc.org/data/g02202/yersions/5).

#### Code availability

Analysis was performed using the Climate Data Operators command line tool (https://code.mpimet.mpg.de/projects/cdo/), Python Programming Language (https://www.python.org/), MATLAB-Climate data tool<sup>64</sup>. The codes used for the present analysis are obtained from the corresponding author upon request.

Received: 7 January 2025; Accepted: 26 April 2025; Published online: 10 May 2025

#### References

- Hoteit, I. et al. Towards an End-to-End Analysis and Prediction System for Weather, Climate, and Marine Applications in the Red Sea. Bull. Am. Meteorological Soc. 102, E99–E122 (2021).
- Zittis, G. et al. Climate Change and Weather Extremes in the Eastern Mediterranean and Middle East. Rev. Geophysics 60, 1–48 (2022).
- Attada, R. et al. The role of the Indian Summer Monsoon variability on Arabian Peninsula summer climate. Clim. Dyn. 52, 3389–3404 (2019).
- Dasari, H. P. et al. Analysis of outdoor thermal discomfort over the Kingdom of Saudi Arabia. GeoHealth 5, e2020GH000370 (2021).
- Lelieveld, J. et al. Model projected heat extremes and air-pollution the eastern Mediterranean and Middle East in the twenty-first century. Regional Environ. Change 14, 1937–1949 (2014).
- Lelieveld, J. et al. Strongly increasing heat extremes in the Middle East and North Africa (MENA) in the 21st century. *Climatic Change* 137, 245–260 (2016).
- Tyrlis, E. & Lelieveld, J. Climatology and dynamics of the summer etesian winds over the Eastern Mediterranean. *J. Atmos. Sci.* 70, 3374–3396 (2013).
- Rama Krishna, K. et al. Investigation of dust-induced direct radiative forcing over the Arabian Peninsula based on high-Resolution WRF-Chem simulations. J. Geophys. Res.: Atmos. 129, 1–22 (2024).
- Lelieveld, J. et al. Climate change and impacts in the Eastern Mediterranean and the Middle East. Clim. Change 114, 667–687 (2012).
- Tyrlis, E., Lelieveld, J. & Steil, B. The summer circulation over the eastern Mediterranean and the Middle East: influence of the South Asian monsoon. Clim. Dyn. 40, 1103–1123 (2013).
- Cherchi, A., Annamalai, H., Masina, S. & Navarra, A. South Asian Summer Monsoon and the Eastern Mediterranean Climate: The Monsoon–Desert Mechanism in CMIP5 Simulations. *J. Clim.* 27, 6877–6903 (2014).
- Cherchi, A. et al. Twenty-first century projected summer mean climate in the Mediterranean interpreted through the monsoon-desert mechanism. Clim. Dyn. 47, 2361–2371 (2016).
- 13. Rodwell, M. J. & Hoskins, B. J. Monsoons and the dynamics of deserts. Q. J. R. Meteorol. Soc. 122, 1385–1404 (1996).
- Capua, D., Tyrlis, E. & Donner, R. V. Tropical and mid-latitude causal drivers of the eastern Mediterranean Etesians during boreal summer. Clim. Dyn. 62, 9565–9585 (2024).
- Chaim, I. G. et al. Precursors of summer heat waves in the Eastern Mediterranean. Q. J. R. Meteorol. Soc. 150, 3757–3773 (2024).
- 16. Yu, Y. et al. Climatology of summer Shamal wind in the Middle East. *J. Geophys. Res.: Atmospheres* **121**, 289–305 (2016).
- Attada, R. et al. Prominent mode of summer surface air temperature variability and associated circulation anomalies over the Arabian Peninsula. Atmos. Sci. Lett. 19, 1–7 (2018).
- Perkins, S. E. & Lewis, S. C. Increasing trend in regional heatwaves. Nat. Commun. 11, 3357 (2020).
- Hoerling, M. et al. On the increased frequency of Mediterranean drought. J. Clim. 25, 2146–2161 (2012).

- Saharwardi, M. D. et al. Long-Term variability in the Arabian Peninsula droughts driven by the Atlantic Multidecadal Oscillation. *Earth's*. *Future* 11. 1–10 (2023).
- Abdelkader, M. et al. Dust–air pollution dynamics over the eastern Mediterranean. Atmos. Chem. Phys. 15, 9173–9189 (2015).
- Gkikas, A., Hatzianastassiou, N., Mihalopoulos, N. & Torres, O. Characterization of aerosol episodes in the greater Mediterranean Sea area from satellite observations (2000–2007). *Atmos. Environ.* 128, 286–304 (2016).
- Shalev, B. et al. Characterization of Eastern Mediterranean dust storms by area of origin; North Africa vs. Arabian Peninsula. *Atmos. Environ.* 198, 158–165 (2019).
- Harikishan, G. et al. Major changes in extreme dust events dynamics over the Arabian Peninsula during 2003–2017 driven by atmospheric conditions. J. Geophys. Res.: Atmospheres 125, 1–20 (2020).
- Krishnamurti, T. N. et al. Desert Air Incursions, an Overlooked Aspect, for the Dry Spells of the Indian Summer Monsoon. *J. Atmos. Sci.* 67, 3423–3441 (2010).
- Tyrlis, E., Tymvios, F. S., Christos, G. & Jos, L. The role of blocking in the summer 2014 collapse of Etesians over the eastern Mediterranean. J. Geophys. Res.: Atmospheres 120, 6777–6792 (2015).
- Dasari, H. P. et al. High-resolution climate characteristics of the Arabian Gulf based on a validated regional reanalysis. *Meteorological Appl.* 29, 1–24 (2022).
- Simpson, I. R., Richard, S., Shaw, T. A. & Ting, M. Mediterranean summer climate and the importance of Middle East topography. *J. Clim.* 28, 1977–1996 (2015).
- Mofidi, A. & Zarrin, A. On the existence of summer shamal wind induced by the Zagros Mountains in the Middle East. *Geophys. Res.* Lett. 49, 1–10 (2022).
- 30. Jin, Q. & Wang, C. A revival of Indian summer monsoon. *Nat. Clim. change* **7**, 587–594 (2017).
- Huang, X. et al. The Recent decline and recovery of Indian summer monsoon rainfall: relative roles of external forcing and internal variability. J. Clim. 33, 5035–5060 (2020).
- Vittal, H. et al. Increased future occurrences of the exceptional 2018–2019 Central European drought under global warming. Sci. Rep. 10, 1–10 (2020).
- Watanabe, M. & Kimoto Atmosphere-Ocean thermal coupling in the Northern Atlantic: A positive feedback. Quat. J. R. Meteorological Soc. 126, 3343–3369 (2000).
- Zhang, P. et al. Impact of East Asian Summer Monsoon Heating on the Interannual Variation of the South Asian High. J. Clim. 29, 159–173 (2016).
- Xiang, B. et al. An emerging Asian aerosol dipole pattern reshapes the Asian summer monsoon and exacerbates northern hemisphere warming. Npj Clim. Atmos. Sci. 1–10. https://doi.org/10.1038/ s41612-023-00400-8 (2023).
- 36. Fu, Z. et al. Dynamic pathway linking Pakistan flooding to East Asian heatwaves. *Sci. Adv.* **10**, 1–12 (2024).
- Hu, P. et al. Revisiting the Linkage Between the Pacific–Japan Pattern and Indian Summer Monsoon Rainfall: The Crucial Role of the Maritime Continent. Geophys. Res. Lett. 51, 1–9 (2024).
- 38. Lu, T. et al. Optimal atmospheric heat sources for the interannual variability of south Asian summer monsoon. *Geophys. Res. Lett.* **51**, 1–10 (2024).
- Manney, G. L. & Hegglin, M. I. Seasonal and regional variations of long-term changes in Upper-Tropospheric jets from reanalyses. *J. Clim.* 31, 423–448 (2018).
- Chowdary, J. et al. The Eurasian jet streams as conduits for east Asian monsoon variability. *Curr. Clim. change Rep.* 5, 233–244 (2019).
- Dong, B. et al. Recent decadal weakening of the summer Eurasian westerly jet attributable to anthropogenic aerosol emissions. *Nat. Commun.* 13, 1–10 (2022).

- Knight, J. R. et al. Climate impacts of the Atlantic Multidecadal Oscillation. Geophys. Res. Lett. 33, 1–4 (2006).
- 43. Ehsan, M. A. et al. Atlantic Ocean influence on Middle East summer surface air temperature. *npj Clim. Atmos. Sci.* **3**, 1–8 (2020).
- Dong, B. & Rowan, T. S. Recent Trends in Summer Atmospheric Circulation in the North Atlantic/European Region: Is There a Role for Anthropogenic Aerosols? J. Clim. 34, 6777–6795 (2021).
- 45. Li, Z. et al. AMO footprint of the recent near-surface wind speed change over China. *Environ. Res. Lett.* **19**, 1–12 (2024).
- Chen, S. et al. Atlantic multidecadal variability controls Arctic-ENSO connection. npj Clim. Atmos. Sci. 8, 1–12 (2025).
- Wang, L. et al. Interdecadal Variation of Springtime Compound Temperature-Precipitation Extreme Events in China and Its Association With Atlantic Multidecadal Oscillation and Interdecadal Pacific Oscillation. J. Geophys. Res.: Atmospheres 130, 1–17 (2025).
- Chen, S. et al. Interdecadal Variation in the Impact of Arctic Sea Ice on El Niño-Southern Oscillation: The Role of Atmospheric Mean Flow. J. Clim. 37, 5483-5506 (2024).
- Tang, Q., Zhang, X. & Francis, J. A. Extreme summer weather in northern mid-latitudes linked to a vanishing cryosphere. *Nat. Clim. Change* 4, 1–6 (2014).
- Coumou, D. et al. The influence of Arctic amplification on mid-latitude summer circulation. *Nat. Commun.* 9, 2959 (2018).
- Langodan, S. et al. Winds and waves in the Arabian Gulf: Physics, characteristics and long-term hindcast. *Int. J. Climatol.* 43, 3538–3551 (2023).
- Mohsen, H. et al. Climatology of the Sistan Levar wind: Atmospheric dynamics driving its onset, duration and withdrawal. *Atmos. Res.* 260, 1–20 (2021).
- 53. Harikishan, G. et al. Dust sources over the Arabian Peninsula. *Environ. Res. Lett.* **18**, 1–14 (2023).
- Hans, H. et al. The ERA5 global reanalysis. Q. J. R. Meteorological Soc. 146, 1999–2049 (2020).
- 55. Randles, C. A. et al. The MERRA-2 aerosol reanalysis, 1980 onward. Part I: System description and data assimilation evaluation. *J. Clim.* **30**, 6823–6850 (2017).
- Holton, J. R. & Hakim, G. J. An Introduction to Dynamic Meteorology (Fifth Edition). Academic Press, https://doi.org/10.1016/C2009-0-63394-8 (2013).
- Lee, H., Jeon, W., Lee, W. S. & Lee, H. W. Human-Perceived temperature changes in South Korea and their association with atmospheric circulation Patterns. J. Clim. 34, 1273–1290 (2021).
- 58. Steadman, R. G. A universal apparent temperature. *J. Appl. Meteorol. Climatol.* **23**, 1674–1687 (1984).
- Scott, C. S., Cameron, C. L. & Erik, T. S. A Comparison between station observations and reanalysis data in the identification of extreme temperature events. *Geophys. Res. Lett.* 47, 1–10 (2020).
- Barriopedro, D. et al. Heat Waves: Physical Understanding and Scientific Challenges. Rev. Geophysics 61, 1–54 (2023).
- 61. Chibuke, C. I., Lee, C. C., Silva, A. & Scott, C. S. Evaluating apparent temperature in the Contiguous United States from four reanalysis products using Artificial Neural Networks. *J. Geophys. Res.: Mach. Learn. Comput.* 1, 1–18 (2014).
- 62. Scott, C. S. & Cameron, C. L. Temporal Trends in Absolute and Relative Extreme Temperature Events Across North America. *J. Geophys. Res.: Atmosphere* **123**, 11889–11898 (2018).
- Wallace, J. M. & Hobbs, P. V. Atmospheric Science: An Introductory Survey. 2nd Edition, Elsevier, Amsterdam, 352-353, 357, 367-368. (2006).
- 64. Greene, C. A. et al. The climate data toolbox for MATLAB Geochem. *Geophys. Geosyst.* **20**, 3774–3781 (2019).

#### **Acknowledgements**

This research was supported by the Climate Change Centre at KAUST, an initiative of the National Center for Meteorology (NCM), Kingdom of Saudi Arabia (Ref No: RGC/03/4829-01-01).

#### **Author contributions**

The main manuscript was prepared by H.G., I.H., H.D., T.L., R.A., and W.H.; S.S. and P.A. contributed through data analysis and formal discussions. All authors reviewed and approved the manuscript.

#### **Competing interests**

The authors declare no competing interests.

#### **Additional information**

**Supplementary information** The online version contains supplementary material available at https://doi.org/10.1038/s41612-025-01072-2.

**Correspondence** and requests for materials should be addressed to Ibrahim Hoteit.

**Reprints and permissions information** is available at http://www.nature.com/reprints

**Publisher's note** Springer Nature remains neutral with regard to jurisdictional claims in published maps and institutional affiliations.

Open Access This article is licensed under a Creative Commons Attribution-NonCommercial-NoDerivatives 4.0 International License, which permits any non-commercial use, sharing, distribution and reproduction in any medium or format, as long as you give appropriate credit to the original author(s) and the source, provide a link to the Creative Commons licence, and indicate if you modified the licensed material. You do not have permission under this licence to share adapted material derived from this article or parts of it. The images or other third party material in this article are included in the article's Creative Commons licence, unless indicated otherwise in a credit line to the material. If material is not included in the article's Creative Commons licence and your intended use is not permitted by statutory regulation or exceeds the permitted use, you will need to obtain permission directly from the copyright holder. To view a copy of this licence, visit http://creativecommons.org/licenses/bync-nd/4.0/.

© The Author(s) 2025